Energy & Buildings 271 (2022) 112296

Contents lists available at ScienceDirect

Energy & Buildings

journal homepage: www.elsevier.com/locate/enb

Oversight of radiative properties of coatings pigmented with TiO_2 nanoparticles

C. Dias [a,*], R.C. Veloso [a,b], J. Maia [b], N.M.M. Ramos [b], J. Ventura [a]

[a] IFIMUP, Departamento de Física e Astronomia, Faculdade de Ciências, Universidade do Porto, Rua do Campo Alegre s/n, 4169-007 Porto, Portugal
[b] CONSTRUCT-LFC, Faculdade de Engenharia, Universidade do Porto, Rua Dr. Roberto Frias, 4200-465 Porto, Portugal

ARTICLE INFO

Article history:
Received 22 April 2022
Revised 24 June 2022
Accepted 4 July 2022
Available online 15 July 2022

Keyword:
FDTD
Cooling
Coatings
Nanoparticles
Titanium dioxide (TiO_2)

ABSTRACT

Passive cooling of buildings under sunlight can be achieved by enhanced coating reflectance. Embedding micro/nano-sized objects, such as nanoparticles, in a lossless material like a polymer, may serve the purpose of reflecting the desired spectrum. The knowledge of the behavior of pigments in the infrared region is therefore a critical factor in formulating coatings to specific requirements. Finite-difference time-domain (FDTD) simulations, which can simulate the propagation of electromagnetic waves in a medium, were here used to investigate the influence of nanoparticle additives on coatings reflection and to explore the corresponding working principles to reveal coatings with high level of reflectance. The numerical simulations demonstrate the reflective behavior in the coating material, showing that embedded titanium dioxide (TiO_2) nanoparticles can significantly improve the reflectance of coatings with maximum values of around 0.9 in average and 0.7 in the infrared for 250 nm radius and 50% particle volume fraction. Furthermore, the reflectance improvement saturates around 100 μm coating thickness. The numerical values are also shown to model experimental results.

1. Introduction

A large amount of energy is consumed for the heating and cooling of the interior space of buildings, resulting in substantial energy consumption and greenhouse gas emissions. Thermal comfort in residential buildings has a large influence on the energy demand. According to the EU report in 2018 [1] about 63.6% of the final energy consumption attributed to the residential households (26.1% of the total final energy in European Union) is directed to heating and cooling, for occupant's thermal comfort. One important factor to consider is that the indoor temperature increases when the exterior surfaces are exposed to solar radiation, leading to large refrigeration requirements to maintain the dwellings comfort (Fig. 1). Since infrared radiation (i.e. wavelength higher than 700 nm) accounts for 50% of solar energy reaching the Earth at sea level (inset of Fig. 1), the ability to reflect radiation in this spectral region is critical. On the other hand, the ultraviolet region (200–400 nm) and the visible band (400–720 nm) represent only 5% and 45% of the total solar energy, respectively [2]. One solution for this issue, without external energy inputs, is through insulation methods, such as insulating materials [3], energy storage systems with phase change materials [4] or reflective coatings [5]. The last option is the most convenient and reliable, since reflective coatings can be applied on the surface of the building, not affecting the original properties [6]. In fact, it was already shown that this method can reduce the external surface temperature by over 10°C [7].

Passive daytime radiative cooling under sunlight can be achieved by embedding micro/nano-sized objects into a binder, such as nanoparticles [8], fibers [9] or nanoplates [10] distributed in a lossless material like a polymer, reflecting the desired spectrum. The nanoparticles will act as scattering medium for the incident light, increasing the optical path length in the active layer. The scattering efficiency depends on the particle size [11], interparticle separation and the refractive index contrast between the particles and the embedding medium [12]. Thus, choosing an additive with a high dielectric constant or a support material with a low one is reasonable to obtain a high scattering rate. Some of these reflective coatings are based on organic pigments, which are easily aged, while most inorganic pigments contain hazardous metals (e.g., cobalt, chromium, cadmium), restricted by environmental regulations. On the other hand, titanium dioxide (TiO_2) exhibiting a high dielectric constant is an ideal candidate to be used as thermal coating additive [13].

These coatings can also be pigmented to the desired color and according with the application using different materials (e.g., Cr_2O_3 for green [14], $NiAl_2O_4$ greenish-blue [15], $CoAl_2O_4$ intense blue [16], $NiTiO_3$ yellow [17], $LaFeO_3$ orange [18] and $BiFeO_3$ for

* Corresponding author.
E-mail address: c.dias@fc.up.pt (C. Dias).

https://doi.org/10.1016/j.enbuild.2022.112296
0378-7788/

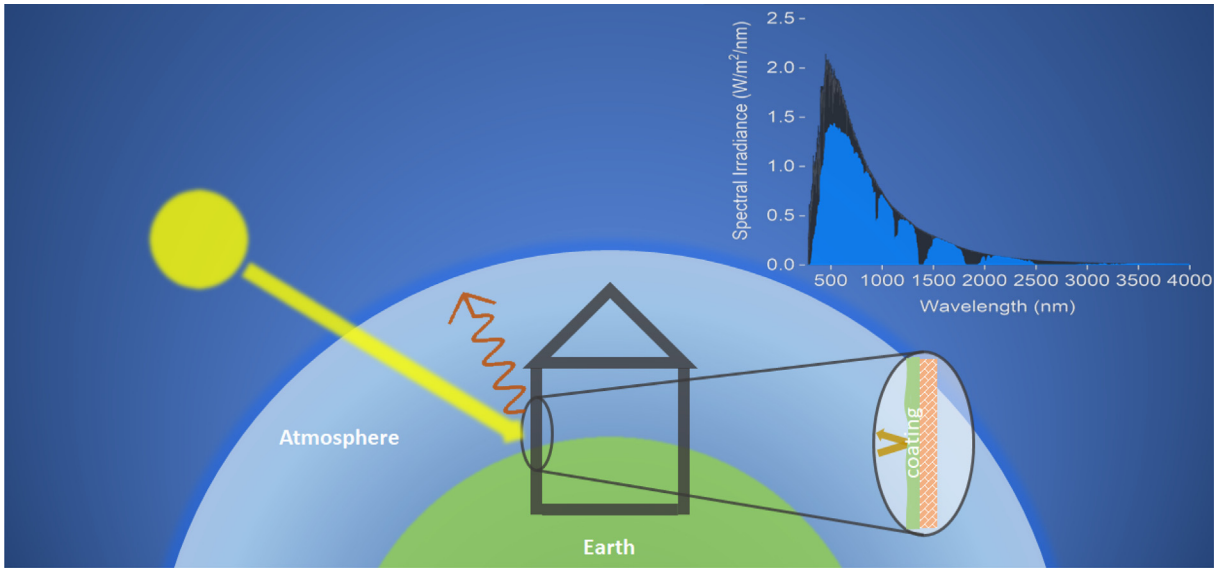

Fig. 1. Schematic diagram of a building with reflective coating under sunlight. The inset shows the solar radiation spectrum at the top of the atmosphere (black) and filtered at sea level (blue) [Solar spectral irradiance at air mass 1.5 (AM 1.5) collected from American Society for Testing and Materials (ASTM). Standard: ASTM G-173-03].

dark brown [19]). Knowledge on the behavior of pigments in the infrared region is a critical factor in formulating coatings to specific requirements [20], so that one must characterize in detail the performance of coatings and nanoparticles [13]. In particular, TiO_2-based materials have attracted a lot of interest from the industry, including the construction sector, due to their unique characteristics, such as high chemical stability, low cost, low toxicity and availability. There are already experimental studies on this subject using TiO_2 nanoparticles as a dopant in coatings [21]. Most studies are focused on the self-cleaning, anti-bacterial, thermal performance and several properties based on its photocatalytic capacity [22,23]. Coatings based on such nanoparticles are already used to reduce the effect of latent heat on the total heat flux in heat pipes [24] and it was shown that implementing a TiO_2-based water film in the external building surface can reduce the surface temperature of the wall by 2 to 7°C [25]. Song et al. studied the particle size distributions of three commercial TiO_2 (280, 360 and 410 nm) pigments and analyzed their influence in the optical properties of acrylic-based coatings [26]. It was observed that, by increasing the particle size, the visible and solar reflectance of the coatings decreased. Piri et al. characterized the spectral reflectance, absorption and transmittance of different substrates coated with TiO_2 nanoparticles with different sizes (35, 120 and 250 nm) and several particle volume fractions (0.1, 0.5, 1, 5 and 10 wt.%), showing that, despite absorbing light in the UV region, TiO_2 nanoparticles reflect the most in VIS and NIR regions [27]. Furthermore, Baneshi et al. investigated the effects of the application of standard (200 nm) and optimized TiO_2 (800 nm) white coatings in a roof to reduce the temperature in buildings [28]. These authors stated that the maximum reduction achieved in annual cooling load demand was of approximately 37% for 200 nm and 31% for 800 nm TiO_2. Shen et al. also observed that higher content of nanoparticles result in greater reflectance and thermal insulation, as well as improved wash resistance and film adhesion [29].

The finite-difference time-domain (FDTD) method is a widely used technique for solving Maxwell's equations at different points in space [12,30]. This is specially relevant when the size of the scattering particles is comparable to the wavelength of the light (Mie scattering solution). Furthermore, it is a proven and stable technique in a broad range of frequencies with smaller computational cost. Some simulation works already explored nanoparticle combinations (TiO_2+SiC) on black painted aluminum [31], titanium oxide and carbon black double-layer nanoparticles [32], TiO_2 with ZnO [33] and TiO_2 with/without voids in a polymer [34] and acrylic [35].

However, to our knowledge, no systematic study involving both particle radius and particle volume fraction has been performed. Thus, here, numerical analyses were performed to predict the reflective properties of nanoparticle-dispersed polymers considering the effects of major factors such as particle size, particle volume fraction and layer thickness. The objective of this study is to use FDTD to characterize the reflective performance of coatings with different additive properties in order to evaluate the best conditions to obtain a high reflective coating. The performances of homogeneous acrylic and acrylic with TiO_2 (nanoparticles) coatings are obtained and critically compared. The influence of the size and particle volume fraction of these nanoparticles, as well as coating thickness, on the total reflectance is studied as a major step in providing guiding instructions for novel designs of optimized reflective coating materials. We further compare our results with experimental measurements.

2. Methodology

The finite-difference time-domain (FDTD) method was implemented using MEEP [36]. The FDTD method divides space and time into a finite rectangular grid, with second-order accuracy, storing different field components at different grid locations. This discretization is known as a Yee lattice and Meep automatically performs a linear interpolation of the field components and stores them for different grid locations. Although simulations of three dimensional (3D) structures provide more reliable results, because of the computational cost, and since this problem involves static isotropic (spherical/cylindrical) objects and the propagation of light coming from the vertical direction, which is invariant in the longitudinal direction, being the results identical at any 2D cross section, we performed two dimensional (2D) FDTD simulations with transverse electric (TE) polarization. This implies that the exact values here obtained cannot be directly compared with experimental measurements, but the overall tendency is valid. Two models were constructed to represent the homogeneous and the TiO_2-embedded acrylic coatings, as shown by the schematic drawing in Fig. 2(a). The acrylic paint is described by a block (*xy*-plane; gray color) with

relative dielectric constant equal to 2.5 [Fig. 2(b)]. The TiO_2 particles are defined by spheres (orange color) with relative dielectric constant equal to 9 (giving a refractive index contrast of $m = \sqrt{9/2.5} \simeq 1.9$). A Gaussian source (red line), representing the incident light,is placed above the acrylic block with downward propagation (y-direction). The top and bottom boundaries (y-direction) of the simulation box are set as perfect matching layer (PML; oblique lines) to absorb electromagnetic waves, simulating a semi-infinite substrate. The left and right boundaries (x-direction) are set as periodic (vertical dashed lines), to simulate an infinite surface. A flux counter is placed on the top surface of the block (blue line), to calculate the reflected radiation. The reflectance is independent of the height of both the source and the flux recorder, provided that the latter is between the block and the source. The simulation is performed for wavelengths ranging from 300 to 2500 nm (solar spectrum) with a resolution of 50 pixels/μm. The nanoparticles are randomly placed inside the acrylic. Each result shown here results from the average of 2–3 simulations for statistical accuracy, with an oscillation on average below 5% between them.

As it is common for simulations involving solar radiation, the reflectance/transmittance spectra was computed using the standard procedure involving two separate calculations: the first to obtain the input power and the second for the scattered power. This means that an initial simulation is run with only air in the FDTD cell medium to calculate the incident flux and, afterwards, the reflected flux is calculated with the complete structure, as it is represented in the flowchart of Fig. 2(c). The reflectance (R) is calculated by dividing the reflected flux ($\phi_{reflected}$) over the incident flux ($\phi_{incident}$), as

$$R = \frac{\phi_{reflected}}{\phi_{incident}}. \quad (1)$$

Note that the reflected/transmitted power can be obtained by simply multiplying the reflectance/transmittance (a fractional quantity) by the solar spectrum (a dimensionless quantity; inset of Fig. 1). For clarity, we show here just the reflectance results.

3. Results

3.1. Coating thickness

Fig. 3 shows the reflectance for different coating thicknesses (1 μm–1 mm) with and without nanoparticles. As expected, the

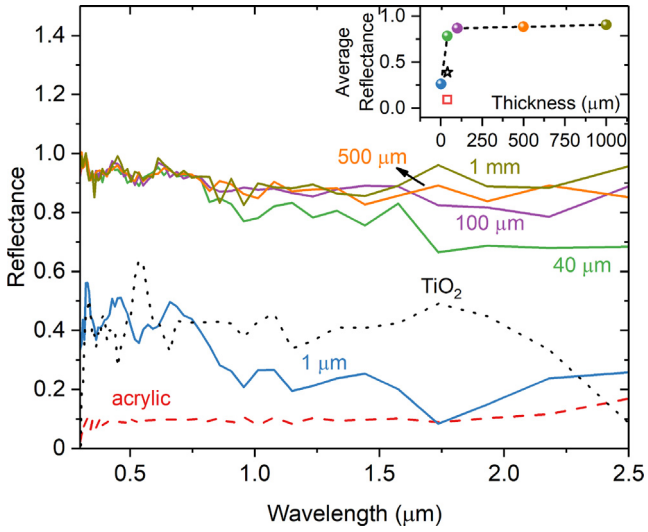

Fig. 3. Reflectance as a function of coating thickness without nanoparticles (acrylic and TiO_2 homogeneous medium) and for nanoparticles of 100 nm radius at a fixed particle volume fraction of 20%. The inset shows the average reflectance as a function of the coating thickness [open symbols for the homogeneous acrylic (square symbol) and TiO_2 (star symbol) layers].

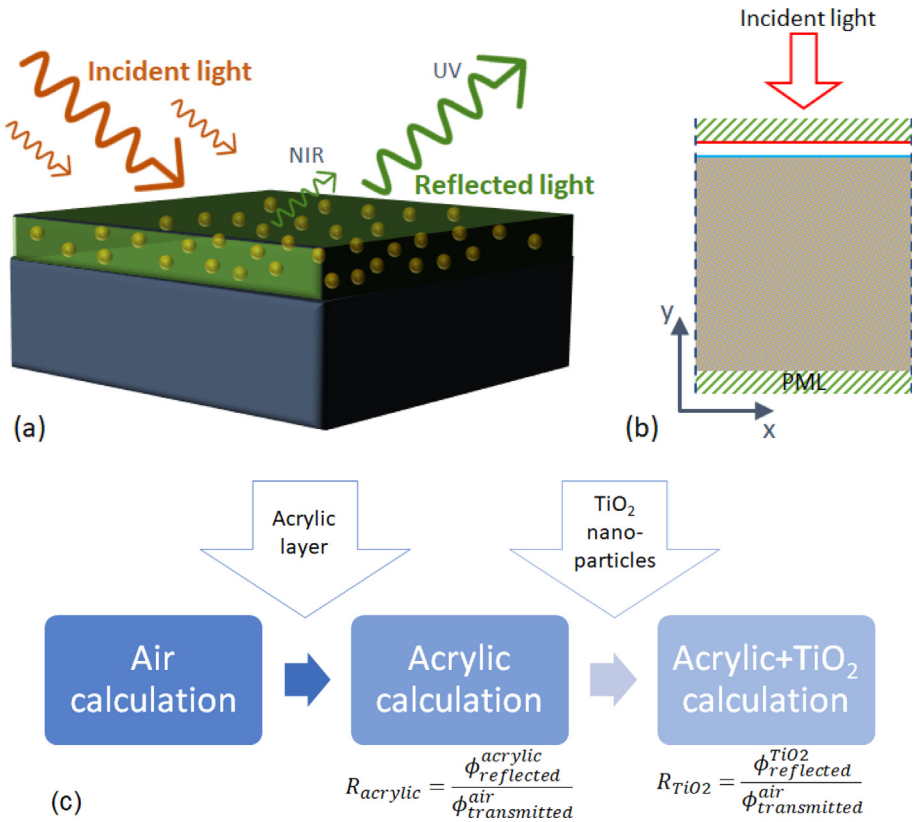

Fig. 2. Schematic diagram of (a) a pigmented coating using spherical/circular nanoparticles, (b) the 2D FDTD cell (cross-section), and (c) the flowchart of the simulation steps.

reflectance without nanoparticles (homogeneous acrylic or TiO_2 layers) is independent of the thickness (dashed and dotted lines shows all the overlapping curves). Note that, as the simulations were performed in 2D, the reflectance does not match the analytical results arriving from the solution of the Fresnel equations (approximately 0.25), since the light source does not include all polarization components, only the *P* polarization (TE mode; approximately 0.15). Nevertheless, we consider this method to be a good compromise between computational resources and qualitative behaviors. The introduction of TiO_2 nanoparticles in the acrylic layer (100 nm radius at a fixed particle volume fraction of 20%) immediately leads to the increase of the reflectance. It is interest-

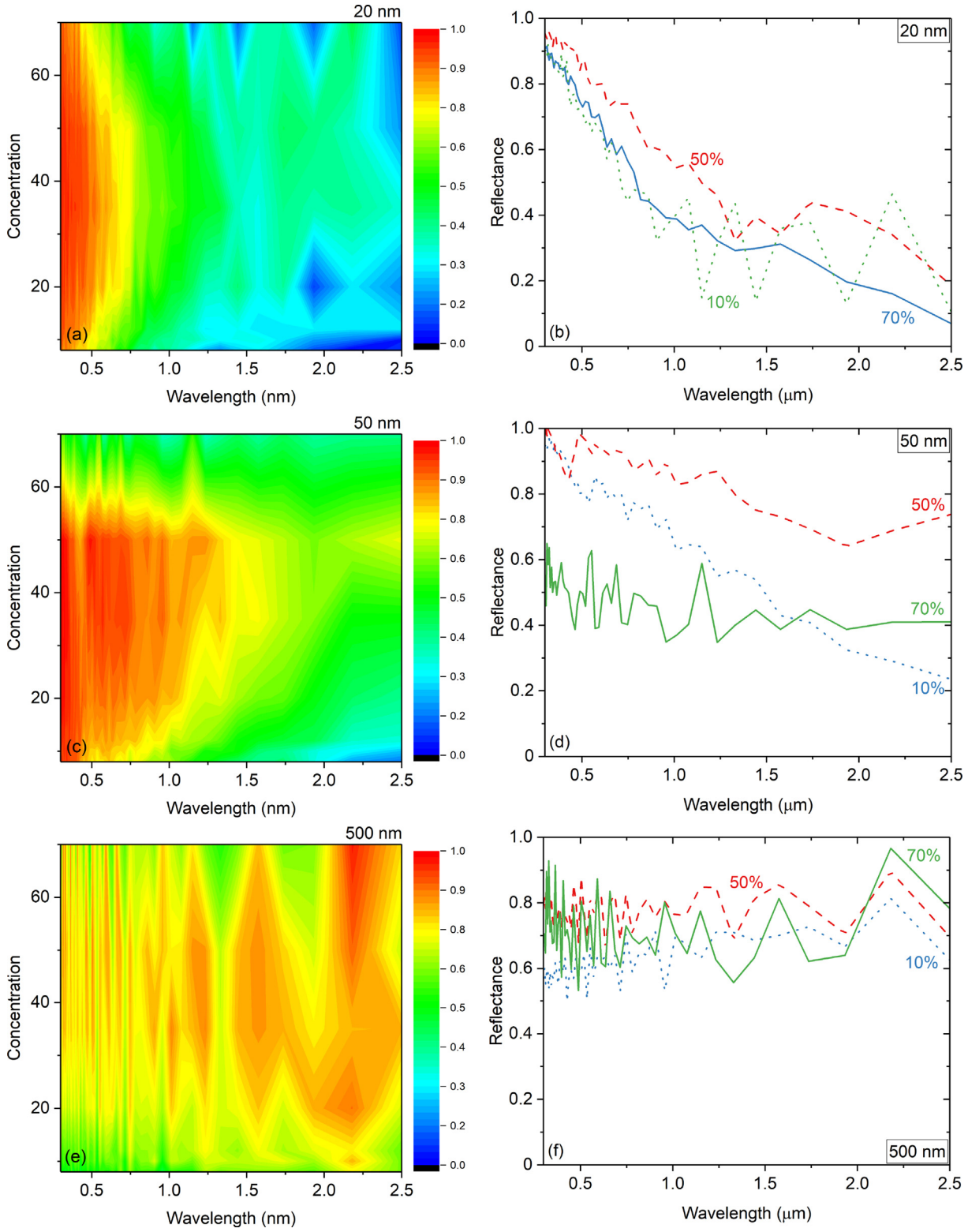

Fig. 4. Reflectance as a function of the wavelength for nanoparticles of radius (a,b) 20 nm, (c,d) 50 nm and (e,f) 500 nm at different particle volume fractions (8, 10, 12, 20, 35, 50 and 70%).

ing to note that the reflectance of the homogeneous TiO_2 layer is higher than that of the thinner coating (1 μm) with TiO_2 nanoparticles, but for the same thickness (40 μm), the nanoparticles result in a reflectance increase of more than two times.

Overall, we observe that the reflectance increases with increasing coating thickness up to a maximum value (100 μm), after which it remains constant in average, as also observed by the saturation in the calculated average reflectance (inset of Fig. 3). This shows that the reflectance cannot be continuously increased simply by increasing the coating thickness. A possible explanation for this is the increase in the absorption due to the higher scattering path or even an increase in transmittance due to multiple scattering. An increase of the reflectance with the increase of TiO_2 pigmented coatings thickness was indeed experimentally observed up to 40 μm [37,38].

3.2. Particle size and volume fraction

To probe how the optimum reflection at different wavelengths depends on the particle size, we performed a systematic study of the reflectance as a function of nanoparticle radius, for different particle volume fractions. The radius of the TiO_2 nanoparticles ranged from 20 nm to 2.5 μm at particle volume fractions of 8, 10, 12, 20, 35, 50 and 70%, relatively to the acrylic content for a 40 μm total thickness.

These results are shown in Fig. 4 in the form of 2D heatmaps [Figs. 4(a,c,e)] for 20, 50 and 500 nm radius nanoparticles, where high reflectances are represented in warm colors and low reflectances in cold colors. We also highlight three particle volume fractions with different behaviors [Figs. 4(b,d,f)], namely a low particle volume fraction (10%) with low reflectance, the particle volume fraction with maximum reflectance (50%) and a particle volume fraction above this value (70%).

From Figs. 4(a,c,e) we see that the smaller particles (20 and 50 nm radius) have higher reflectances at lower wavelengths, corresponding mainly to the UV and VIS regions, whereas the maximum reflectances for the 500 nm radius particles is shifted to the IR region. Looking at the complete spectrum, larger nanoparticle sizes ensure reflectances always above 0.5, while reflectance can be as low as 0.1 (similar to the case without nanoparticles), for the smaller sizes at high wavelengths. This increase of the reflectance in the IR region with the nanoparticle size increase is in agreement with the experimental results obtained for TiO_2 coatings from a few dozen nanometers up to the micrometer diameter scale [26,27,37,39,40]. All the represented sizes show a maximum reflectance at a particle volume fraction of 50%, decreasing after that value [Figs. 4(b,d,f)].

We performed the same study for larger nanoparticles (100 nm, 250 nm and 2.5 μm radius) at 10, 20, 50 and 70% (Fig. 5). For these radius and particle volume fractions the reflectance is rather constant in the entire spectrum, with the bigger particles (2.5 μm) always showing a lower reflectance and the 250 nm radius showing the higher overall reflectance. Having the 500 nm radius as a comparison point [Figs. 4(e,f)], a slight increase is observed for 250 nm at all particle volume fractions, but the 100 nm and 2.5 μm cases show a progressive decrease.

It is interesting to note that, independently of the radius, the reflectance steadily increases with particle volume fraction up to 50%. The same overall trend was also experimentally observed although up to 30 wt% likely due to agglomeration [26,39]. For example, an increase on the volume fraction of 500 nm nanoparticles from 10 to 50% represents a gain in the reflectance of 20% (0.6 to 0.8). For the largest particles (2.5 μm) the same increase is observed, but at lower reflectance magnitudes (0.3 to 0.5). This larger radius shows the smaller reflectance for all particle volume fractions, which indicates that the nanometer range is better for reflectance improvement.

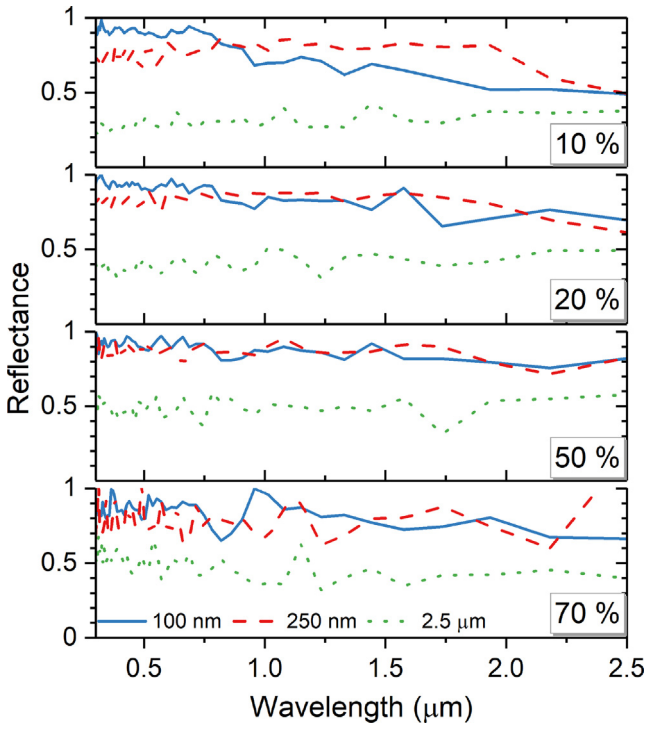

Fig. 5. Reflectance as a function of the wavelength for different nanoparticles radius (100, 250 and 2500 nm) and particle volume fractions (10, 20, 50 and 70%).

3.3. Average reflectance and color

To better quantify the reflectance, the integral over the entire spectrum divided by the wavelength range gives us the average reflectance as

$$R_{average} = \frac{\int_{0.3}^{2.5} R(\lambda) d\lambda}{0.3 - 2.5}, \tag{2}$$

where λ is the wavelength and the average reflectance, $R_{average}$, is calculated for the complete range (0.3–2.5 μm). To take into account the solar spectral irradiance [AM 1.5; $L(\lambda)$], we also calculated the weighted reflectance over a certain wavelength range ($\lambda_{min} - \lambda_{max}$) as

$$R_{weighted} = \frac{\int_{\lambda_{min}}^{\lambda_{max}} R(\lambda) L(\lambda) d\lambda}{\int_{\lambda_{min}}^{\lambda_{max}} L(\lambda) d\lambda}, \tag{3}$$

for UV (0.3–0.4 μm), VIS (0.4–0.7 μm) and IR (0.7–2.5 μm) regions.

The integral over a certain wavelength range divided by the overall spectrum integral (0.3–2.5 μm) gives the percentage of the total reflectance in that range

$$R_{\%} = \frac{\int_{\lambda_{min}}^{\lambda_{max}} R(\lambda) d\lambda}{\int_{0.3}^{2.5} R(\lambda) d\lambda}. \tag{4}$$

These quantities are shown in Figs. 6(a) and 6(b), respectively. The horizontal lines in the left panel of Fig. 6(a) show the reflectances for the case of homogeneous acrylic and TiO_2 mediums (no nanoparticles). Also, the reflectance of homogeneous mediums with intermediate dielectric constants would be enclosed between those of the homogeneous TiO_2 and acrylic layers (not shown). It is clear that the presence of the TiO_2 nanoparticles in the acrylic matrix always results in an improved reflectance above 10% particle vol-

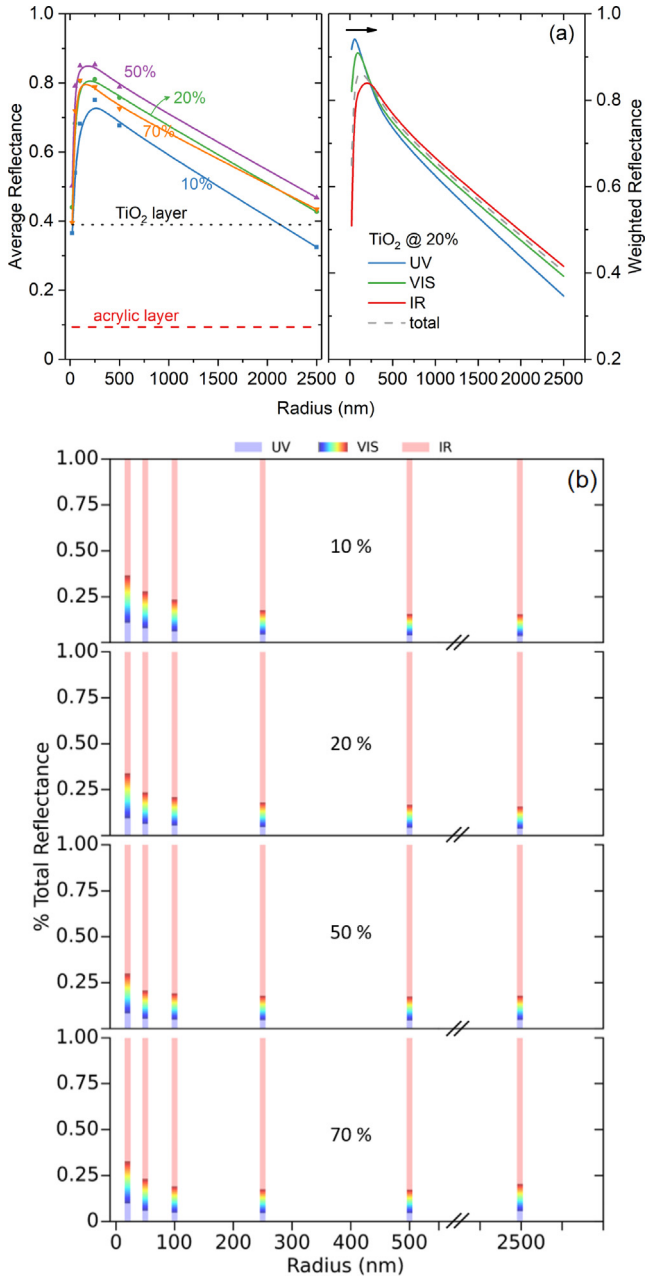

Fig. 6. (a) Total averaged reflectance (including homogeneous acrylic and TiO_2 layers; left) and UV, VIS and IR weighted at 20% particle volume fraction (right) as a function of particle radius. (b) Partial UV, VIS and IR reflectances as a function of the nanoparticle radius and particle volume fraction (10, 20, 50 and 70%).

ume fraction and even at 10% except for 20 nm and 2.5 μm radius. We observe that, for all particle volume fractions, the maximum in the average reflectance is obtained for the 100–250 nm radius range. The overall maximum of the average reflectance (0.85) is achieved at 50% TiO_2 particle volume fraction. This is also the case for the IR region. For all the cases, the IR region is the biggest parcel of the average reflectance [Fig. 6(b)]. Namely, for all particle volume fractions it represents between 63% (smaller radius) and 85% (larger radius) of the overall reflectance. Furthermore, as expected, we observed how the particle size influences the optimum reflection region. As shown in the right panel of Fig. 6(a) for fixed 20% particle volume fraction and previously mentioned, the maximum of the weighted reflectance shifts to bigger nanoparticle radius when the radiation wavelength increases. For instance, UV shows a maximum at 50 nm radius and IR at 200 nm. This is also clear in Fig. 6(b) from

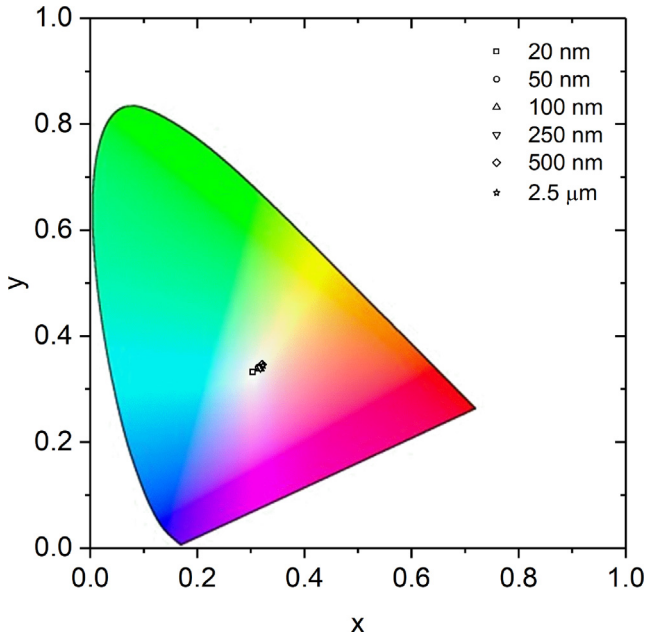

Fig. 7. Color coordinates of pigmented coatings for different radius at 20% particle volume fraction.

the blue bar (UV) being larger for the smaller radius (left) and the red bar (IR) being larger for bigger radius (right).

Finally, the CIE (International Commission on Illumination) colorimetric system was used for color analysis of the coating, for eye comfort, aesthetic or camouflage applications. The color coordinates are plotted on the chromaticity diagram of Fig. 7 for the different radius at 20% particle volume fraction. As shown, TiO_2 pigments produce a mostly white color for all particle sizes, as expected being TiO_2 a white pigment. No differences were observed for different particle volume fractions at fixed radius.

4. Discussion and validation

We observed that the thickness of the coating influences the reflectance as seen in Fig. 3, with a lower limit (∼1 μm) where a homogeneous TiO_2 layer shows higher reflectance than nanoparticles doping and a higher limit (100 μm) where the reflectance saturates. The size of the nanoparticles shifts the wavelength of the maximum reflectance, being larger nanoparticles (hundreds of nm) indicated to maximize the reflectance in the desired IR spectrum range (Figs. 4–6). Similarly, the particle concentration increases the reflectance up to a limit (50%), where there is a balance between the binding medium and the dopant (Figs. 4 and 5). The obtained white color in the CIE system (Fig. 7) is in accordance with the expected for an acrylic and TiO_2 mixture and the obtained high reflectance values.

To validate our study, we performed experimental measurements to compare with our simulations. Commercial rutile TiO_2 nanoparticles from US Nano with 250 nm radius were dispersed on a 5% w/w PMMA and toluene solution at 3, 16 and 40% w/w, then spin coated at 1000 rpm for 30 s three times on glass substrates and finally dried at 80°C overnight (inset of Fig. 8). A modular spectrophotometer [FLAME-T (UV–vis) and FLAME-NIR (NIR)] from Ocean Optics was used to measure the reflectance in the 200–1650 nm region, which was averaged from three measurements at different locations for each sample. Both experimental and numerical results show very similar reflectivity values and the same overall increasing trend in the total and IR reflectances with the concentration (Fig. 8). This clearly demonstrates that our numeri-

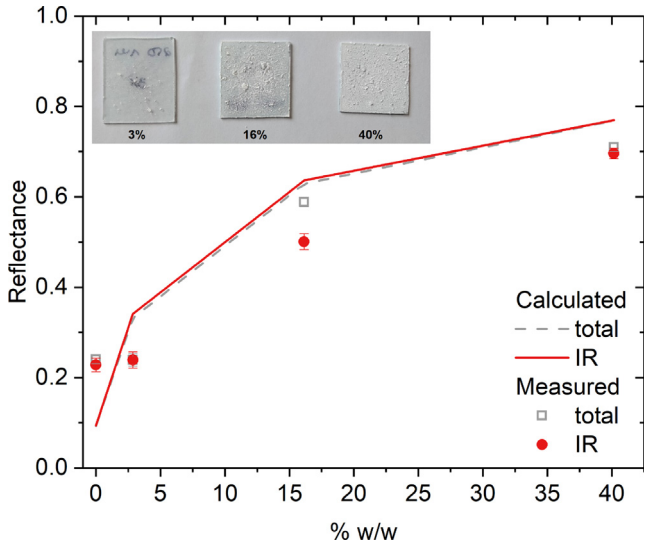

Fig. 8. Experimental and simulated total and IR reflectance on 3, 16 and 40% w/w TiO_2@PMMA coatings with 250 nm radius rutile. The inset shows the optical images of the prepared coatings.

cal model is able to predict the reflectance of a medium doped with nanoparticles and describe its dependence on the nanoparticle concentration.

5. Conclusions

This work studied in detail an approach to increase light reflectance in coatings, decreasing the cooling demands in buildings by pigmenting them with TiO_2 nanoparticles. We have numerically analyzed the proposed structure with the FDTD method, using MEEP. We observed that the reflectance cannot be increased by simply increasing the thickness of the doped coating, with a saturation after 100 μm. In order to achieve the maximum enhancement in light reflectance we varied both particle size and particle volume fraction. The maximum in the reflection shifts to bigger particle size as the wavelength increases. We obtained optimum results at 250 nm radius of TiO_2 nanoparticles and 50% particle volume fraction for a maximum reflectivity of 0.95 (0.9 average reflectance and 0.7 in the IR). Therefore, as typical commercial titanium dioxide pigments are manufactured with a particle size of 200 nm, they may be a good option with an optimum near-infrared reflectance.

These results were validated by experimental measurements and give a detailed guideline to formulate new coatings with increased near-infrared reflectance of buildings façades. From here, a study of the influence of particle radius distribution from commercial suppliers on the reflectance can be pursuit. Furthermore, the mixing between different nanoparticle materials (e.g., TiO_2 and CuO) can balance the quest to find both high reflective and non-white coatings.

Declaration of Competing Interest

The authors declare that they have no known competing financial interests or personal relationships that could have appeared to influence the work reported in this paper.

Acknowledgments

This work was financially supported by Project PTDC/ECI-CON/28766/2017—POCI-01–0145-FEDER-028766 funded by FEDER through COMPETE2020—Programa Operacional Competitividade e Internacionalização (POCI) and by national funds (PIDDAC) through FCT/MCTES, Project Circular2B - 37_CALL#2 - Circular Construction in Energy-Efficient Modular Buildings financing under the Environment, Climate Change and Low Carbon Economy Programme within the scope of the European Economic Area Financial Mechanism EEA Grants 2014-2021 and by Base Funding—UIDB/04708/2020 of the CONSTRUCT—Instituto de I&D em Estruturas e Construções—funded by national funds through the FCT/MCTES (PIDDAC). R. C. Veloso would like to acknowledge the support of FCT - Fundação para a Ciência e a Tecnologia for the funding of the Doctoral Grant SFRH/BD/148785/2019.

References

[1] European Union. Directive (EU) 2018/844 of the European Parliament and of the Council of 30 May 2018 Amending Directive 2010/31/EU on the Energy Performance of Buildings and Directive 2012/27/EU on Energy Efficiency. 2018;p. 75–91.
[2] ASTM G173. Standard Tables for Reference Solar Spectral Irradiances: Direct Normal and Hemispherical on 37 Tilted Surface. American Standard Test Method.; 2012
[3] W. Villasmil, L.J. Fischer, J. Worlitschek, A review and evaluation of thermal insulation materials and methods for thermal energy storage systems, Renewable Sustain. Energy Rev. (2019) 71–84.
[4] M.H. Zahir, S.A. Mohamed, R. Saidur, F.A. Al-Sulaiman, Supercooling of phase-change materials and the techniques used to mitigate the phenomenon, Appl. Energy 240 (2019) 793–817.
[5] R.C. Veloso, A. Souza, J. Maia, N.M.M. Ramos, J. Ventura, Nanomaterials with high solar reflectance as an emerging path towards energy-efficient envelope systems: a review, J. Mater. Sci. 56 (36) (2021) 19791–19839.
[6] J. Mandal, Y. Yang, N. Yu, A.P. Raman, Paints as a Scalable and Effective Radiative Cooling Technology for Buildings, Joule 4 (7) (2020) 1350–1356.
[7] N.M.M. Ramos, J. Maia, A.R. Souza, R.M.S.F. Almeida, L. Silva, Impact of Incorporating NIR Reflective Pigments in Finishing Coatings of ETICS, Infrastructures 6 (6) (2021) 79.
[8] W. Li, Y. Li, K.W. Shah, A materials perspective on radiative cooling structures for buildings, Solar Energy 207 (2020) 247–269.
[9] R.A. Yalçın, E. Blandre, K. Joulain, J. Drévillon, Daytime radiative cooling with silica fiber network, Solar Energy Mater. Solar Cells 206 (July) (2020).
[10] P. Li, A. Wang, J. Fan, Q. Kang, P. Jiang, H. Bao, et al., Thermo-Optically Designed Scalable Photonic Films with High Thermal Conductivity for Subambient and Above-Ambient Radiative Cooling, Adv. Funct. Mater. 32 (5) (2022) 2109542.
[11] N. Sangiorgi, L. Aversa, R. Tatti, R. Verucchi, A. Sanson, Spectrophotometric method for optical band gap and electronic transitions determination of semiconductor materials, Opt. Mater. 64 (2017) 18–25.
[12] V. Mann, V. Rastogi, FDTD simulation studies on improvement of light absorption in organic solar cells by dielectric nanoparticles, Optical Quant. Electron. 52 (5) (2020) 1–16.
[13] A. Zhou, Z. Yu, C.L. Chow, D. Lau, Enhanced solar spectral reflectance of thermal coatings through inorganic additives, Energy Build. 138 (2017) 641–647.
[14] R. Levinson, P. Berdahl, H. Akbari, Solar spectral optical properties of pigments–Part II: survey of common colorants, Solar Energy Mater. Solar Cells 89 (4) (2005) 351–389.
[15] S.G. Menon, H.C. Swart, Microwave-assisted synthesis of blue-green NiAl2O4 nanoparticle pigments with high near-infrared reflectance for indoor cooling, J. Alloys Compounds 819 (2020) 152991.
[16] A.A. Ali, E. El Fadaly, I.S. Ahmed, Near-infrared reflecting blue inorganic nano-pigment based on cobalt aluminate spinel via combustion synthesis method, Dyes Pigments 158 (2018) 451–462.
[17] A. Moghtada, A. Shahrouzianfar, R. Ashiri, Facile synthesis of NiTiO3 yellow nano-pigments with enhanced solar radiation reflection efficiency by an innovative one-step method at low temperature, Dyes Pigm. (2017) 388–396.
[18] L. Liu, A. Han, M. Ye, M. Zhao, Synthesis and characterization of Al3+ doped LaFeO3 compounds: A novel inorganic pigments with high near-infrared reflectance, Solar Energy Mater. Solar Cells 132 (2015) 377–384.
[19] L. Yuan, A. Han, M. Ye, X. Chen, L. Yao, C. Ding, Synthesis and characterization of environmentally benign inorganic pigments with high NIR reflectance: Lanthanum-doped BiFeO3, Dyes Pigments 148 (2018) 137–146.
[20] M. Baneshi, S. Maruyama, H. Nakai, A. Komiya, A new approach to optimizing pigmented coatings considering both thermal and aesthetic effects, J. Quantitative Spectrosc. Radiat. Transfers 110 (3) (2009) 192–204.
[21] Z. Song, W. Zhang, Y. Shi, J. Song, J. Qu, J. Qin, et al., Optical properties across the solar spectrum and indoor thermal performance of cool white coatings for building energy efficiency, Energy Build. 63 (2013) 49–58.
[22] J.O. Carneiro, G. Vasconcelos, S. Azevedo, C. Jesus, C. Palha, N. Gomes, et al., The evaluation of the thermal behaviour of a mortar based brick masonry wall coated with TiO2 nanoparticles: An experimental assessment towards energy efficient buildings, Energy Build. 81 (2014) 1–8.
[23] M. Janczarek, Ł. Klapiszewski, P. Jędrzejczak, I. Klapiszewska, A. Ślosarczyk, T. Jesionowski, Progress of functionalized TiO2-based nanomaterials in the

construction industry: A comprehensive review, Chem. Eng. J. 430 (2022) 132062.
[24] W.N. Septiadi, G.A. Iswari, P.B. Sudarsana, G.J.P. Putra, D. Febraldo, N. Putra, et al., Effect of Al2O3 and TiO2 nano-coated wick on the thermal performance of heat pipe, J. Therm. Anal. Calorim. (2021).
[25] J. He, A. Hoyano, A numerical simulation method for analyzing the thermal improvement effect of super-hydrophilic photocatalyst-coated building surfaces with water film on the urban/built environment, Energy Build. 40 (6) (2008) 968–978.
[26] J. Song, J. Qin, J. Qu, Z. Song, W. Zhang, X. Xue, et al., The effects of particle size distribution on the optical properties of titanium dioxide rutile pigments and their applications in cool non-white coatings, Solar Energy Mater. Solar Cells (2014) 42–50.
[27] N. Piri, A. Shams-nateri, J. Mokhtari, Solar spectral performance of nanopigments, Solar Energy Mater. Solar Cells 162 (2017) 72–82.
[28] M. Baneshi, S. Maruyama, The impacts of applying typical and aesthetically-thermally optimized TiO2 pigmented coatings on cooling and heating load demands of a typical residential building in various climates of Iran, Energy Build. 113 (2016) 99–111.
[29] L. Wei Shen, Y. Mei Zhang, P. Gen Zhang, J. Jie Shi, Z. Ming Sun, Effect of TiO2 pigment gradation on the properties of thermal insulation coatings, Int. J. Miner., Metall. Mater. 23 (12) (2016) 1466–1474.
[30] J. Feng, M. Santamouris, Numerical techniques for electromagnetic simulation of daytime radiative cooling: A review, AIMS Mater. Sci. 6 (6) (2019) 1049–1064.
[31] H. Bao, C. Yan, B. Wang, X. Fang, C.Y. Zhao, X. Ruan, Double-layer nanoparticle-based coatings for efficient terrestrial radiative cooling, Solar Energy Mater. Solar Cells 168 (February) (2017) 78–84.
[32] Z. Huang, X. Ruan, Nanoparticle embedded double-layer coating for daytime radiative cooling, Int. J. Heat Mass Transfer 104 (2017) 890–896.
[33] J. Chai, Q. Cheng, M. Si, Y. Su, Y. Zhou, J. Song, Numerical simulation of white double-layer coating with different submicron particles on the spectral reflectance, J. Quant. Spectrosc. Radiat. Transfer 189 (2017) 176–180.
[34] J.P. Bijarniya, J. Sarkar, P. Maiti, Performance simulation of polymer-based nanoparticle and void dispersed photonic structures for radiative cooling, Sci. Rep. 11 (1) (2021) 1–14.
[35] M. Baneshi, S. Maruyama, A. Komiya, The effects of using some common white pigments on thermal and aesthetic performances of pigmented coatings, J. Therm. Sci. Technol. 4 (1) (2009) 131–145.
[36] A.F. Oskooi, D. Roundy, M. Ibanescu, P. Bermel, J.D. Joannopoulos, S.G. Johnson, Meep: A flexible free-software package for electromagnetic simulations by the FDTD method, Comput. Phys. Commun. 181 (3) (2010) 687–702.
[37] M. Baneshi, H. Gonome, A. Komiya, S. Maruyama, The effect of particles size distribution on aesthetic and thermal performances of polydisperse TiO 2 pigmented coatings: Comparison between numerical and experimental results, J. Quant. Spectrosc. Radiat. Transfer 113 (8) (2012) 594–606.
[38] H. Lu, M. Huang, K.S. Shen, J. Zhang, S.Q. Xia, C. Dong, et al., Enhanced Diffuse Reflectance and Microstructure Properties of Hybrid Titanium Dioxide Nanocomposite Coating, Nanoscale Res. Lett. 13 (2018).
[39] M. Baneshi, S. Maruyama, A. Komiya, The effects of TiO2 pigmented coatings characteristics on temperature and brightness of a coated black substrate, Solar Energy 86 (1) (2012) 200–207.
[40] Q. Gao, X. Wu, Y. Fan, Solar spectral optical properties of rutile TiO2 coated mica-titania pigments, Dyes Pigments 109 (2014) 90–95.